Acta Geotechnica
https://doi.org/10.1007/s11440-024-02347-3

RESEARCH PAPER

Morphology characterization of unsaturated soils under drying-wetting cycles: crack opening and closure

Zhuang Zhuo[1,2] · Weiling Cai[1] · Cheng Zhu[1] · Chao-Sheng Tang[3] · Kaniz Roksana[1]

Received: 13 September 2023 / Accepted: 18 April 2024

Abstract

The volumetric and hydrological responses of clayey soils subjected to drying-wetting (D-W) cycles are of paramount importance for the integrity of geoenvironmental infrastructures. The study aimed to investigate the cracking behavior of clayey soils under D-W cycles by using advanced 2D imaging and 3D scanning techniques to capture the initiation and propagation of desiccation cracks within a soil specimen. The temporal variation in the soil water content and the corresponding 2D digital photography and 3D morphology of cracks were simultaneously monitored, and the cracking characteristics were interpreted. It was found that the time-dependent evaporation process was independent of the D-W cycles. Both 2D and 3D characterization showed the cracking hysteresis phenomenon in the unsaturated soil, which indicates the dependency of the crack opening and closure on the degree of saturation. D-W cycles led to the formation of subcracks and the increase in the total crack length, reflecting the soil degradation. Additionally, it was demonstrated that the 3D characterization exhibited the advantage of capturing the volumetric change and the subtle change in the macro-porosity of the cracked soil over the 2D visualization. The current study provides a perspective of combining 2D and 3D characterization for interpreting the volumetric change of cracked soils and enhancing the understanding of the hydromechanical responses and the soil-atmosphere interactions.

Keywords 3D structured light scan · Desiccation cracking · Image processing · Quantitative soil cracking analysis · Wetting–drying cycles

1 Introduction

Desiccation cracking is induced by the excess drought stress that might deteriorate the subsurface soils [34, 48]. Numerous studies have shown that the initiation and propagation of desiccation cracks can have adverse effects on the mechanical and hydraulic properties of the soil, which might undermine the safety and serviceability of geoenvironmental infrastructures [8, 13, 19, 20, 25, 35]. As a result, the long-term performance of many engineering structures, such as landfill liners and covers, geological waste disposal facilities, earth embankments, and road pavements, may be degraded due to the tensile failure and volumetric expansion of cracked soils [1, 4, 7, 21, 37]. Therefore, there are increasing research interests and imperative needs on characterizing the morphology of the desiccation crack and the associated volumetric change in the soil during the desiccation process.

In-situ soils typically undergo diurnal fluctuations and periodic drying-wetting (D-W) cycles [34]. The D-W cycles can alter both hydraulic and mechanical properties of the soil by disturbing the pore structure (i.e., physical soil degradation). Previous studies [16, 24, 39] have shown that the permeability of soil samples generally increased significantly after the first D-W cycle, although there are conflicting

✉ Cheng Zhu
zhuc@rowan.edu

[1] Center for Research and Education in Advanced Transportation Engineering Systems (CREATEs), Department of Civil and Environmental Engineering, Rowan University, 201 Mullica Hill Road, Glassboro, NJ 08028, USA

[2] School of Safety Engineering, North China Institute of Science and Technology, 467 Xueyuan Street, Sanhe 065201, Hebei, China

[3] School of Earth Sciences and Engineering, Nanjing University, 163 Xianlin Avenue, Nanjing 210023, Jiangsu, China

Published online: 12 May 2024

trends between slightly and highly compacted soils after 4 D-W cycles [16]. The soil stiffness has been found to decrease because of D-W cycles in the existing study [30]. Morphological investigations [3, 40, 41] have revealed high repeatability (i.e., crack memory) in the formation of crack patterns (or crack network) during D-W cycles. The crack network tends to reappear in the vicinity of previous cracks, indicating the reactivation of historical failure zones during subsequent D-W cycles. The importance of studying soil behaviors under D-W cycles has been emphasized by the occurrence of extreme weather events and accelerated global climate changes [10, 18].

The initiation of desiccation cracks is primarily triggered by soil shrinkage at the surface defect [27]. Desiccation cracks propagate as the soil volume contracts, driven by air intrusion and suction stress concentrations during desaturation [51]. The correlations between crack characteristics and soil volume changes are therefore the key to the interpretation of hydromechanical properties of cracked soils. Tang et al. [33] investigated the relationship between the crack propagation and the soil shrinkage characteristic curve. It is found that the cracking occurred in the structural, normal, and residual shrinkage stages and terminated at the shrinkage limit [33]. Li and Zhang [13] found that the critical suction value and water content of the desiccation crack initiation could be inferred from the soil–water retention properties and soil shrinkage characteristic curves. Zhao and Santamarina [51] suggested that the nucleation of desiccation cracks should occur at the suction equal to or larger than the air entry value. However, it is worth noting that the presence of desiccation cracks within the soil mass can lead to an overestimation of void ratio, which hinders the accurate measurement of void-ratio-dependent hydromechanical responses (i.e., soil–water retention properties and soil shrinkage characteristics) [46]. Thus, it is of importance to capture the volume change of the cracked soil. However, traditional cracking characteristics are usually obtained by 2-dimensional (2D) image processing [13, 15, 32], which cannot quantify the actual deformation and soil degradation of cracked soils. It is therefore essential to apply the three-dimensional (3D) characterization of desiccation cracks within the soil for interpretation of the soil desiccation process and associated changes in hydromechanical soil properties [11]. The 3D characterization of desiccation cracks could provide information (i.e., cracking depth and nonuniform volume change) that cannot be obtained from 2D images.

Non-destructive imaging techniques are typically used to interpret 3D characteristics of desiccation cracks, such as X-ray computed tomography and 3D laser scanning. The X-ray computed tomography is obtained based on various extents of absorption of X-rays by geomaterials, which can reconstruct the porous structure [38]. The X-ray computed image analyzes facilitate the pore-scale investigation on the granular samples by visualizing the soil pore network, fabric structure, and grain interactions [12, 38]. This allows to exhibit the evolution of macroscopic soil behaviors including capillary collapse [43], desiccation shrinkage [11], crack propagation [6], compression behaviors [44] etc. While the X-ray computed tomography focuses on the internal porous structure of the cracked soil, the 3D laser scanning is acquired using the reflection of the near-infrared light on the soil surface, projecting the morphology of desiccation cracks [52]. Analysis methods such as triangulation method [9] and the 3D digital image correlation method [45] can be aided to the laser scanning technique to interpret the process of desiccation cracking. For instance, Sanchez et al. [26] interpreted the 3D morphology of the desiccation cracks using a 2D profile laser device. In their study, the elevation of a typical cross-section, the crack area, and the specimen volume were analyzed. Zhuo et al. [52] investigated the 3D characterization of clayey soil using a structured light scanner. They developed a postprocessing methodology to calculate the surface area, the specimen volume and the fractal dimension of dried soil samples. As compared with the surface image-based DIC method, 3D characterization techniques yield more details in the visualization of the morphology and pore structure of the cracked soil. However, these methods have not been extensively applied in studies of soil-atmosphere interactions. To the best of the authors' knowledge, few studies have utilized the 3D characterization method to investigate volumetric cracking characteristics and the accompanied desaturation process of the cracked soils under D-W cycles.

The objective of this research is to employ both 2D and 3D characterization techniques to investigate the desiccation cracking process of the clayey soil under D-W cycles. The 2D digital photography and the 3D morphology obtained from a structured light scanner were both utilized to qualify and quantify cracking characteristics. Based on digital imaging processing, the evolution of crack length, crack width, and crack area of the cracked soil under D-W cycles was analyzed. Using the structured light method, the 3D surface morphological features, such as the surface area, the specimen volume and the surface fractal dimension, were interpreted. By combining 2D and 3D methods, a comprehensive analysis of the macroscopic cracking process would be presented and the underlying mechanism of soil degradation due to D-W cycles can be revealed.

2 Material and methodology

2.1 Soil

The clayey soil used in this study was acquired from a local construction site in South Jersey. The physical properties of

Table 1 Physical properties of the soil tested in this study

Soil Properties	Values
Specific gravity	2.68
Liquid Limit (%)	46.4 ± 1.0
Plastic Limit (%)	21.2 ± 1.0
Plasticity Index (%)	25.2 ± 1.0
USUC classification	CL
Sand (0.075–2 mm) (%)	30.2
Silt (0.002–0.075 mm)	35.7
Clay (< 0.002 mm) (%)	34.1
Dominant minerals	Quartz and Gismondine

this soil are summarized in Table 1. According to the Unified Soil Classification System (USCS), the soil can be classified as low-plasticity clay (CL). The soil consists of 30.2% of fine sand and 69.8% of fine-grained soils in which the mineralogy is dominated by gismondine. The liquid limit and plastic limit were found to be 46.5% and 21.1%, respectively. Based on the measured Atterberg limits, the free swelling potential was estimated as 5.0% using the empirical relationship [49].

2.2 Experimental setup

An integrated experimental setup was established to capture the water evaporation process, 2D cracking characteristics, and 3D cracking morphologies of soil samples. A high sensitivity balance with 0.001 g resolution was adopted to record the weight changes of the soil sample. A high-resolution digital camera (Canon EOS Rebel T6i) was adopted to take 2D images of the specimen every 30 min. To capture 3D geometrical features, a structured light 3D scanner system (HP 3D Structured Light Scanner Pro S3) was used to scan the soil every 4 h. Figure 1 presents a schematic view of the experimental setup. The camera and 3D scanner system (includes a scanner and a projector) were positioned above the soil sample. To obtain the 3D morphology information from different observation angles, the soil sample was placed on a rotation table. The rotation table pivoted 60° after the completion of each scanning, with 6 scans from different angles required for each round. Notably, the sample used for 3D scanning was placed on a rotation table, which was fixed in position throughout the experiment to minimize any position change-induced errors. To monitor both the evaporation process and the crack propagation of the soil specimen, two identical soil samples were prepared and tested simultaneously. One was placed on the rotation platform to obtain the crack characteristics and the another was kept on the balance to provide the water content for the cracked soil. This approach of using parallel soil specimens for conducting different measurements simultaneously was adopted from previous studies [2, 31]. The experiment was performed in a chamber with relatively stable environmental conditions (temperature range: 25 °C ± 1 °C; relative humidity range: 50% ± 5%) to avoid the influence of wind and sunlight on the evaporation. To evaluate the potential error introduced by the parallel soil specimen, an extra test was performed by using the same apparatus under the same environmental conditions. Two identical soil samples were placed on two electronic balances, and the mass changes of the two samples were simultaneously recorded during the desiccation cracking every 30 min. According to the

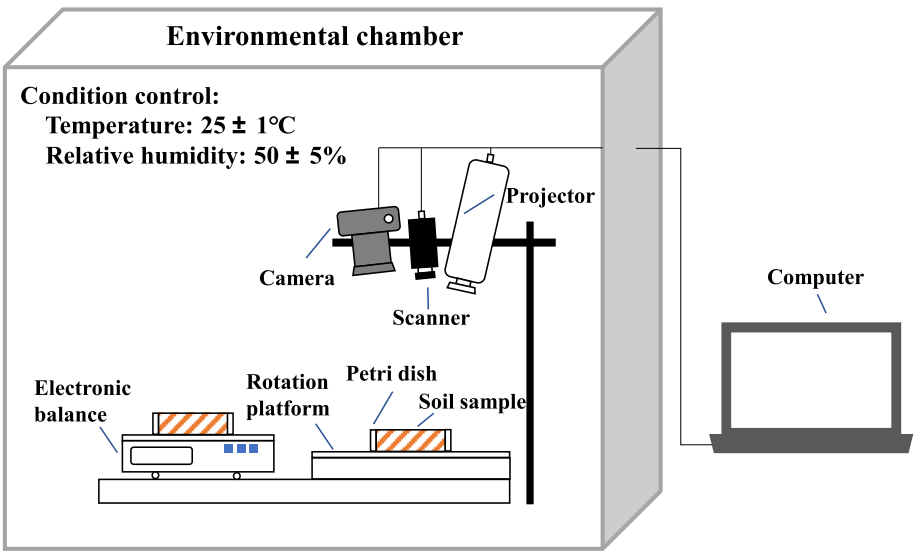

Fig. 1 Schematic view of the experiment setup

monitoring of the sample mass within 120 h, the difference of the mass between two samples was minimum (less than 0.005 g). This indicates that two soil samples could considerably share the same water content measured.

2.3 Test procedure

Figure 2 shows the testing procedure of soil desiccation tests under D-W cycles. Soil samples were prepared by mixing the clayey soil with deionized water to achieve the target water content of 70%, which was approximately 1.5 times the liquid limit to ensure a homogeneous slurry state. Then the slurry was then poured equally into two identical Petri dishes (diameter = 8.4 cm, height = 1.84 cm) to prepare a scanned sample and a parallel sample. Thereafter, two samples were cured for 3 days by covering the top with a lid and plastic membrane. The first drying cycle started when the curing process was completed.

In the current study, 6 D-W cycles were performed and the individual drying and wetting paths were denoted as D1 to D6 and W1 to W6, respectively. Each cycle started with the gravimetric water content of 70% and ended at the same water content of 1%. During the drying process, the weight changes, 2D digital images (one photo per 30 min), and 3D scans (one scan per 4 h) were recorded automatically during the drying process. Each drying process was considered finished when the weight of soil samples remained unchanged for over 24 h.

During the wetting process, distilled water was carefully added by a pipette to the dried soil sample through multiple portions, to restore the soil water content to its original level (70%). This was achieved by controlling and monitoring the gradual changes in the mass on the high-resolution balance. Meanwhile, the slow wetting process should not induce any damage on the surface of the cracked soil as observed in instantaneous 2D and 3D digital images. Restoring the water content to its original level is the reason why such procedure allows the comparison of cracking characteristics in different D-W cycles under the same boundary conditions (i.e., initial water content) [31]. The wetting process was divided into 10 intervals. In each interval (i.e., every 5 min), 2 g of water were added to the soil sample and the uniform distribution of moisture was ensured by using pipette [31]. The weight of the sample was recorded, a photo of the sample was taken and a 3D scan was taken after each addition of 2 g of water. After the target water content was added, the wet sample was cured for 3 days before the next drying process to ensure the complete crack closure. During the process of crack closure, the self-healing capacity of the clayed soil could be observed and the amount of water to alleviate the drought stress could be estimated [31, 50].

2.4 2D image processing

The images taken during the D-W cycles were analyzed with a 2D image processing package named Crack Image Analysis System (CIAS, free available at www.climate-engeo.com). Figure 3 shows the process of digital image processing procedure to obtain the cracking characteristics. Firstly, the original photo (Fig. 3a) was converted into a gray-scale image (Fig. 3b). The gray-scale image can be used to estimate the number of pixels at any point so that cracks can be identified distinguishably, as shown in Fig. 3c. Based on the threshold values (i.e., number of pixels) on the binary image, the algorithm in the CIAS could automatically recognize the crack segments and analyze the crack information (Fig. 3d). The algorithm of recognizing crack segments was based on the cluster analysis method [15] so that the crack network can be extracted to interpret the crack characteristics (e.g., crack propagation, crack number, node number and crack area, etc.). In the current study, the 2D crack characteristics were quantified by the cracking area, the crack ratio (the ratio between the crack area to the total area), the total crack length (the trace length of the medial axis of the crack segment), and the average crack width (the shortest distance from a randomly chosen point on the boundary to the

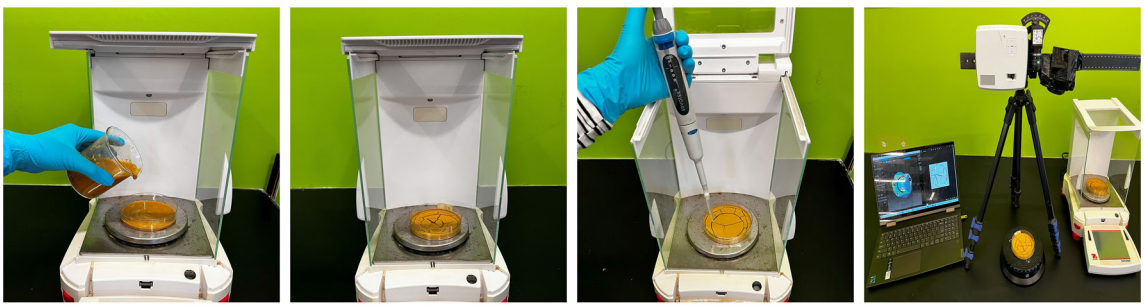

Fig. 2 Test procedures: **a** sample preparation, **b** drying process, **c** wetting process, and **d** 2D and 3D image analyzes

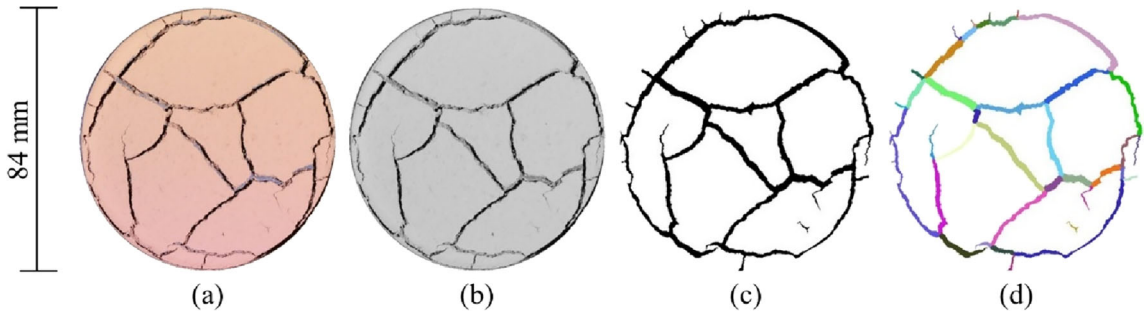

Fig. 3 Digital image processing procedure: **a** original colored image, **b** gray-scale image, **c** binary image, and **d** crack segmentation

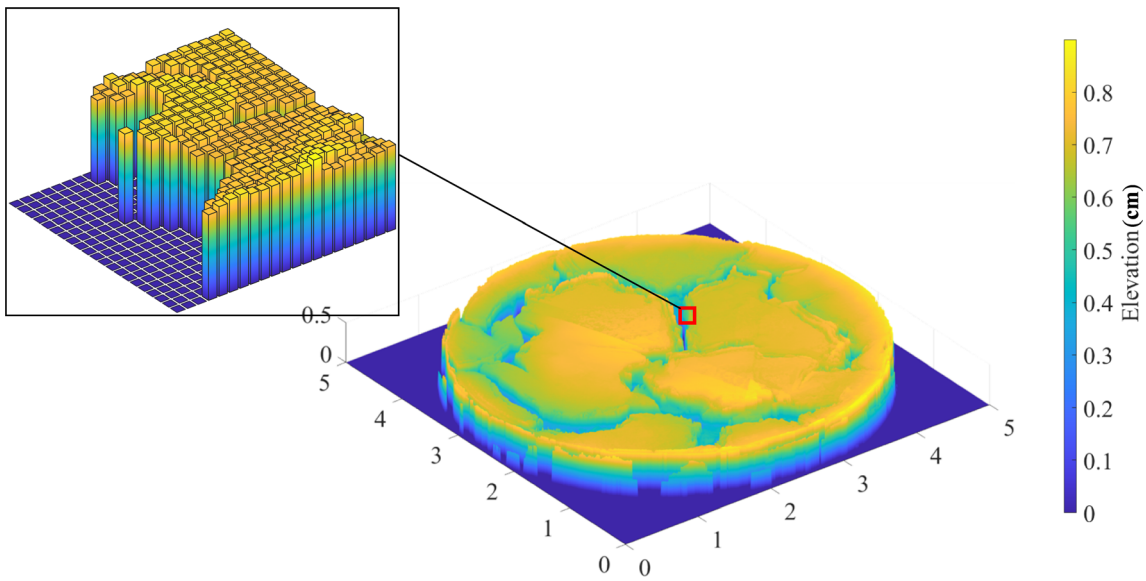

Fig. 4 Example of the reconstructed 3D model with the magnified view of a local volume

crack's opposite boundary) [15]. The resolution of the image used in this method was approximately 9 pixel/mm. More details about this method can be found in [32, 37].

2.5 3D scanning data processing

A 3D laser scanning was adopted in the test to capture the 3D information of the cracked soils, as shown in Fig. 1. The scanner can capture the surface coordinates of the scanned object in the x, y, and z axis. The resulting 3D scans were reconstructed and visualized the cracked soil structure through converting 3D scanning data into a coordinate matrix. The scanned soil mass was discretized into 1000 by 1000 columns according to the planar coordinates (as shown in Fig. 4) and the volume of the non-uniform soil tomography was obtained from the volume integral of each discrete column. With the processed data, it is possible to extract not only the cracking information but also the 3D soil structure information such as soil volume, surface area (the overall surface area of the cracked soil including the soil top surface and the side surface of cracks) and the fractal dimension of the cracked soil surface. The resolution of the 3D laser scanning in this study was approximately 6 pixel/mm in all three axes. Further details on the date inversion of the 3D scanning process can be found in our previous research [51].

3 Results and discussion

3.1 Water evaporation

Water evaporation is the driving factor that governs the initiation and evolution of desiccation cracks. It has been found that the water evaporation process depends on both soil properties (e.g., water content, mineralogy, and microstructure) [34, 47] and environmental conditions (e.g., wind speed, temperature and relative humidity) [22]. The variation in environmental conditions might affect the thermodynamics between the soil–water-air interface,

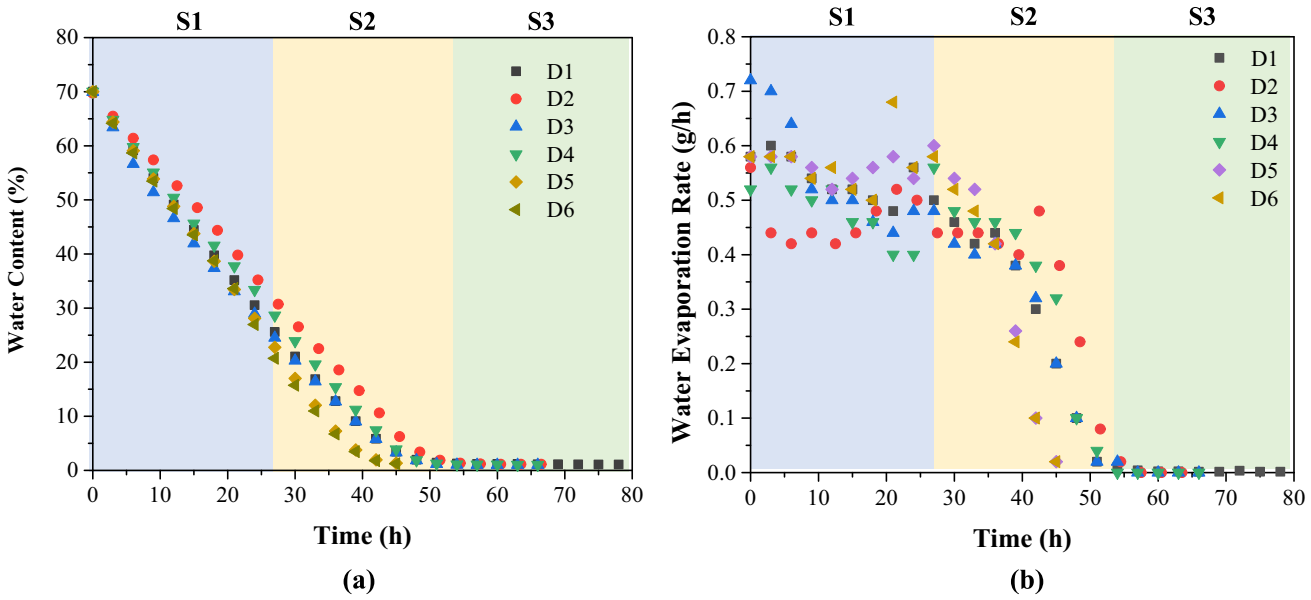

Fig. 5 The temporal evolution of water loss in the drying path in 6 D-W cycles (D1-D6): **a** water content changes and **b** water evaporation rate changes

leading to the change in the evaporation process. The temporal desiccation process of the soil specimens during 6 D-W cycles was captured by monitoring the water content and evaporation rate (refer to Fig. 5). In general, the tendency of evaporation for the soil was unaffected by D-W cycles. As indicated in Fig. 5a, the water content decreased steadily during the first 30 h, then the evaporation rate reduced from 30 to 50 h and finally stabilized after 50 h.

The evaporation process of soil specimens can be characterized by three stages [34, 42], namely constant rate stage (S1), falling rate stage (S2), and residual rate stage (S3), as shown Fig. 5b. In the first stage (i.e., S1), where the capillary action dominates, soils remain saturated and the evaporation rate is maintained at its maximum level. In the falling rate stage (i.e., S2), soils become unsaturated and the soil suction increases rapidly, leading to a decrease in evaporation rate. Toward the end of the drying process (i.e., S3), the water retention of soils is governed by the water absorbed, which hinders the desaturation and minimizes evaporation rates. Generally, the constant rate stage (S1) varied from 0 to 27th hour; the falling rate stage (S2) continued from 27 to 54th hour; and the residual rate stage (S3) went from 54 to 80th hour. The evolution of water evaporation rates in six cycles followed similar trends (Fig. 5b).

3.2 2D characterization of desiccation cracks

Driven by the evaporation, the initiation and propagation of the crack network of the soil showed the dependency on the water content. Cracks started to appear during the constant rate stage as shown in Fig. 5. It was noticed that the first cracks in all six drying processes were all initiated in the first stage. The crack initiation and propagation in the 2D crack network of the soil under 6 D-W cycles were analyzed. It should be noted that the crack network was fully developed during the drying path, while the wetting process healed the soil cracking. In each D-W cycle, the emergence of the first crack on the soil specimen was captured and the corresponding water content was measured, as shown in Fig. 6.

The first crack was captured when the CIAS recognized the crack segment based on the instantaneous digital images [15]. It was shown that the water content at the emergence of the first crack increased due to wetting–drying cycles. This suggests that the crack resistance of the soil subjected to wetting–drying cycles decreases, leading to the occurrence of desiccation cracks at a higher degree of saturation. This finding is consistent with previous studies [23, 32]. This phenomenon might be explained by the soil degradation which causes the permanent deformation on the soil macrostructure and consequently triggers the desiccation crack easily [29]. However, in the current study, it should be also noticed that the crack initiation from D2 to D6 was triggered at a lower water content. This might be attributed to the fact that with the increasing number of wetting–drying cycles, more desiccation cracks were formed. That caused an increase in the exposed area for evaporation, leading to a decrease in water content at the occurrence of the first crack [22]. This explanation might not be supported by 2D crack characteristics since the total exposed area for evaporation cannot

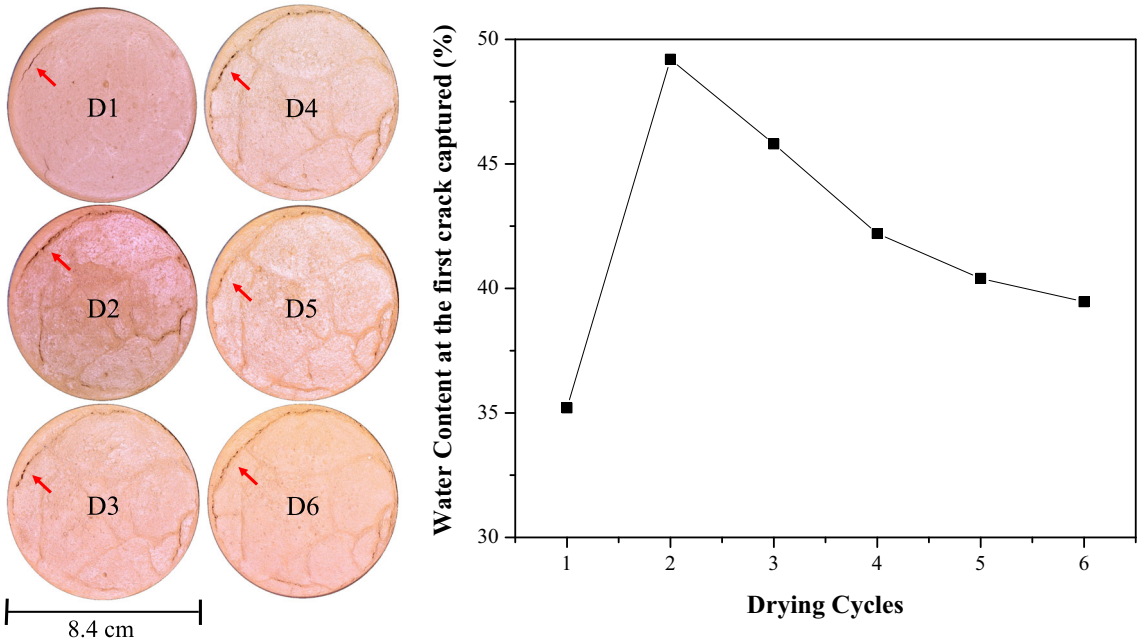

Fig. 6 2D-images showing the crack initiation and the corresponding water content

be obtained from 2D images. In fact, this could be verified by the 3D characterization which is discussed in the following section.

The typical crack network of the soil is shown in Fig. 7. Overall, the pattern of the crack network remained unaltered during D-W cycles. However, some subcracks (marked by red arrow in Fig. 7) were generated during D-W cycles. As compared to the crack network in D1, three subcracks were generated in D2. With a further increase in D-W cycles, the generation of subcracks was reduced in D3 and D4 and no subcracks are formed after 5 D-W cycles. This finding indicates that D-W cycles induce soil degradation by triggering more subcracks within the soil [2] and this deterioration would be stabilized after a certain number of D-W cycles. It highlights the importance of applying sufficient D-W cycles in the desiccation test to

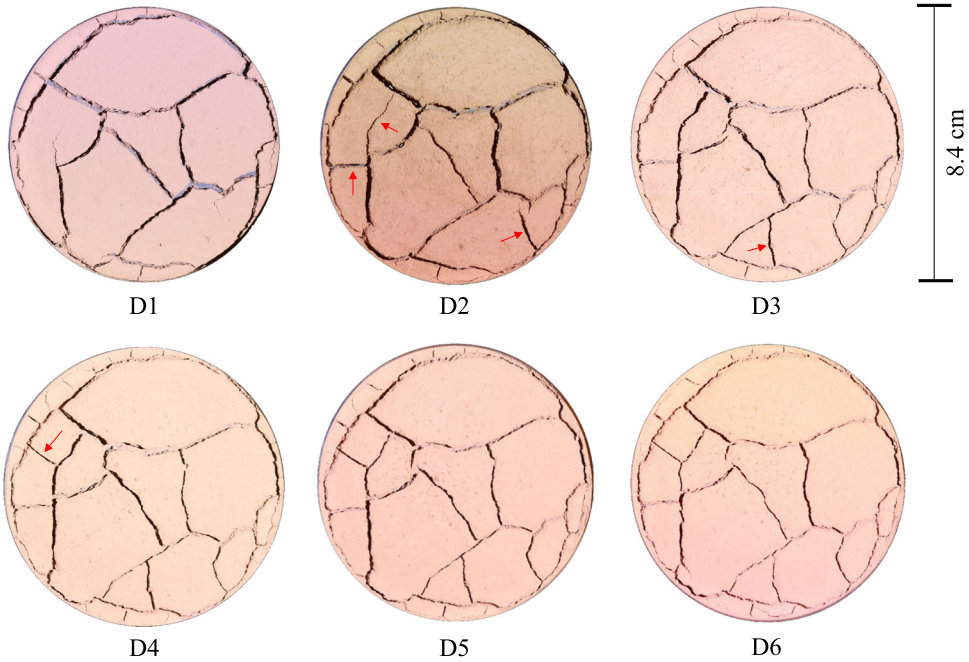

Fig. 7 2D Cracking network in the drying path of 6 D-W cycles

determine the terminal fabric structure of the cracked soil and assess its long-term hydromechanical properties.

The above description of desiccation cracks was based on qualitative visual observations. The geometry of cracks, as shown in Fig. 7, was extracted and quantified by 2D characteristics of crack segments (e.g., the total crack length, average crack width, and crack ratio). Figure 8 presents the evolution of crack length with the water content in the drying path in 6 D-W cycles. The crack length increased dramatically within the constant rate stage and gradually stabilizes in the following two stages, as shown in Fig. 5. Due to D-W cycles, the final crack length at the end of the drying path increased from 60.5 cm (D1) to 71.3 cm (D4), and then remained nearly unchanged from D4 to D6, which agrees with the visual observation in Fig. 7. It was also found that the crack length increased with a decrease in the water content. This further confirms that the initiation and propagation of desiccation cracks are driven by the desaturation and air invasion [27, 51]. The comparison of total crack length between wetting and drying paths is presented in Fig. 8b. A hysteresis phenomenon existed where, at the same water content, the total crack length in the drying path was consistently larger than that in the wetting path. This indicates that the crack opening in the drying path and the crack closure in the wetting path achieve different crack intensities under the same water content level. This phenomenon was consistent with the hydraulic hysteresis in soil water retention curves [14]. The suction stress in the drying path was higher than that of the wetting path for a given degree of saturation, which explains more crack opening and less crack closure at the same water content [13]. This implies that the behaviors of crack opening and closure could be characterized by the soil water retention curves in D-W cycles.

The variation of the average crack width against the water content is shown in Fig. 9. In contrast to the evolution of the total crack length, the final average crack width decreased with the number of cycles. Similar experimental results were found by [40]. Notably, the average crack width continually decreased after the fourth D-W cycle from 0.130 to 0.076 cm, even though the total number of cracks and the total crack length remained nearly unchanged. It seems that the self-healing capacity of desiccated clay would increase with D-W cycles, but this result contradicts the conclusion of soil degradation induced by D-W cycles. It might be explained by the macroporosity loosening during D-W cycles, leading to the reduction in macropore size and the associated crack width [29]. This finding also suggests that the crack width based on the 2D characterization might not be a suitable indicator for representing the degradation of the pore structure of the cracked soil. Furthermore, the evolution of the average crack width in each D-W cycle followed a similar trend as the total crack length (Fig. 9b). Under the same water content, the average crack width in the wetting process was smaller than that in the drying process, indicating the hysteresis of crack opening and closure in D-W cycles.

Knowing the total crack length and the average crack width, the crack area was correspondingly computed and interpreted by the crack ratio, as shown in Fig. 10. The crack ratio generally decreased with the D-W cycle, as shown in Fig. 10a. This might not necessarily disagree with the soil degradation due to D-W cycles. While in the individual wetting or drying paths, the crack ratio increased with a decrease in the water content (Fig. 10b). This indicates the crack-induced damage of the soil structure and suggests that 2D characterization could not considerably capture the influence of D-W cycles on the soil structure, despite showing the sensitivity to the water content.

The pronounced hysteresis phenomenon of cracking in D-W cycles is shown by the evolution of all 2D cracking characteristics. The 2D visualization of cracking hysteresis is presented using the sample at the fourth D-W cycle. Figure 11 presents the 2-D images of the soil sample on both wetting and drying paths at various water content levels. Specifically, the images indicate that at relatively low (1%, 7%, 13%, 20%) and relatively high (56%, 63%, 70%) water contents, the crack pattern and soil surface in the drying and wetting paths were very similar. However, at meddle water contents such as 26%, 32%, and 38%, the crack width and crack area in the wetting path were less than that in the drying path. This was probably caused by the hydraulic hysteresis of water retention characteristics which provides a lower suction stress on the wetting path than that on the drying path under a same degree of saturation or water content [13, 14]. The temporal evolution of 2D cracking characteristics showed the process of crack opening and closure (i.e., self-healing capacity) which was governed by the soil–water retention responses (i.e., hydraulic hysteresis). The quantified 2D cracking characteristics (from Figs. 8, 9 and 10) captured the self-healing phenomenon of the soil, which showed that at the water content of about 40% on the wetting path, the desiccation crack was completely close. It seems that the soil could be completely healed; however, the crack network (referring to Figs. 7 and 10) retained its cracking memory, indicating the incomplete crack healing [5, 50]. It should be noted that the self-healing capacity of the soil is highly dependent on the plasticity index and the swell potential [5]. The soil used in the current study had a low swell potential (i.e., 5%), representing a considerably poor self-healing capacity [5, 49]. It should be noted that these 2D images could not characterize the volumetric change of the cracked soil and the total exposed area of the soil to the atmosphere. To fully understand the influence of desiccation cracks on the

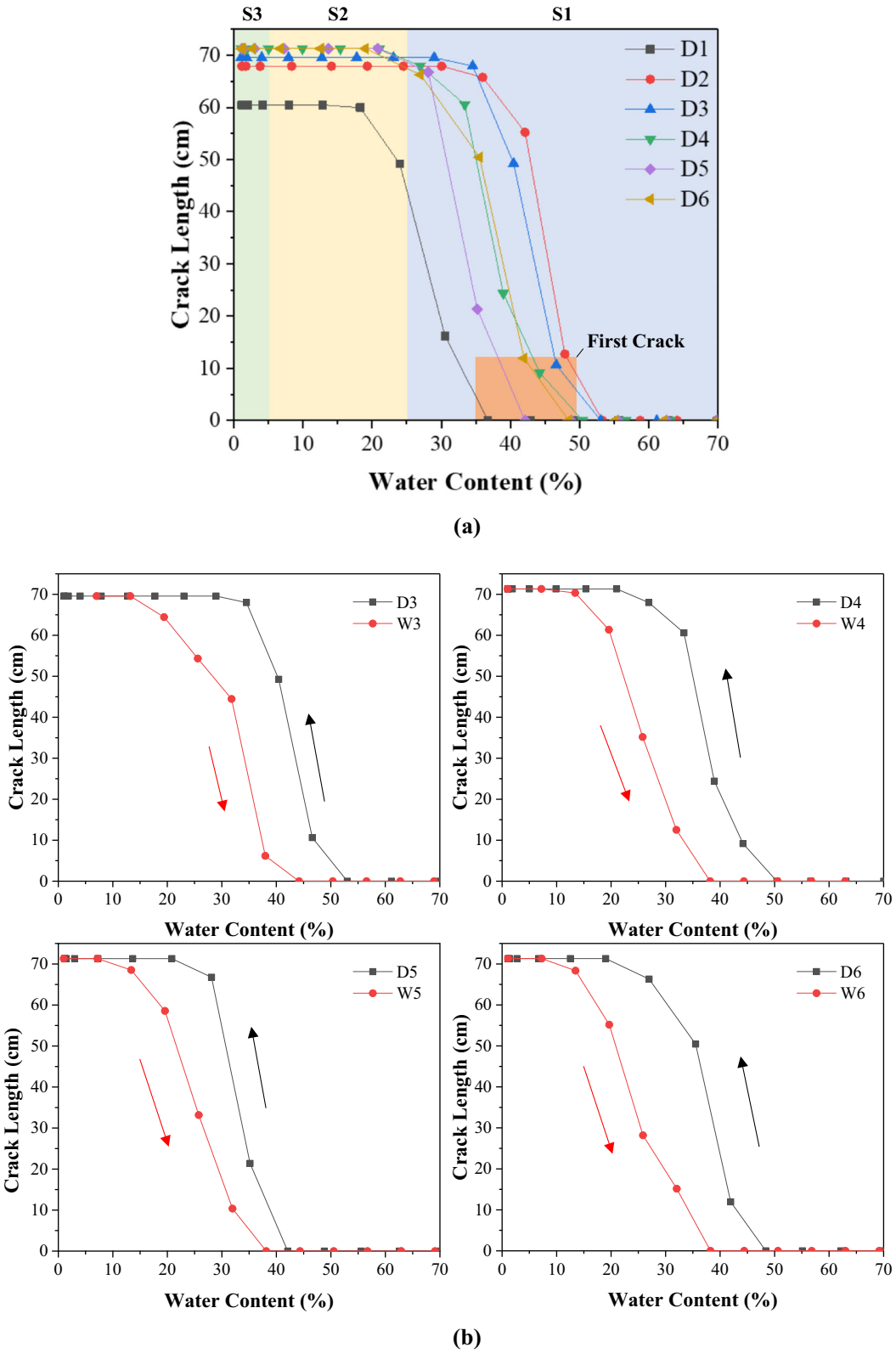

Fig. 8 **a** The evolution of the crack length with water content in 6 drying paths and **b** the comparison of the crack length between wetting and drying paths in D-W cycles

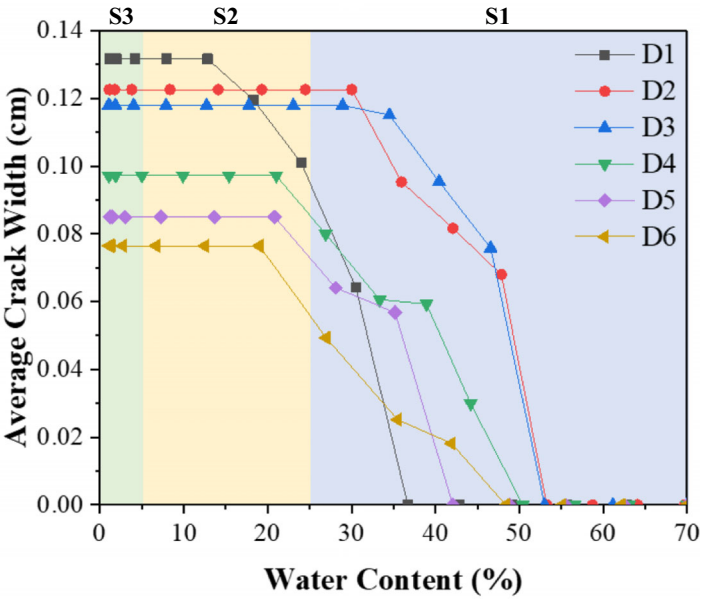

(a)

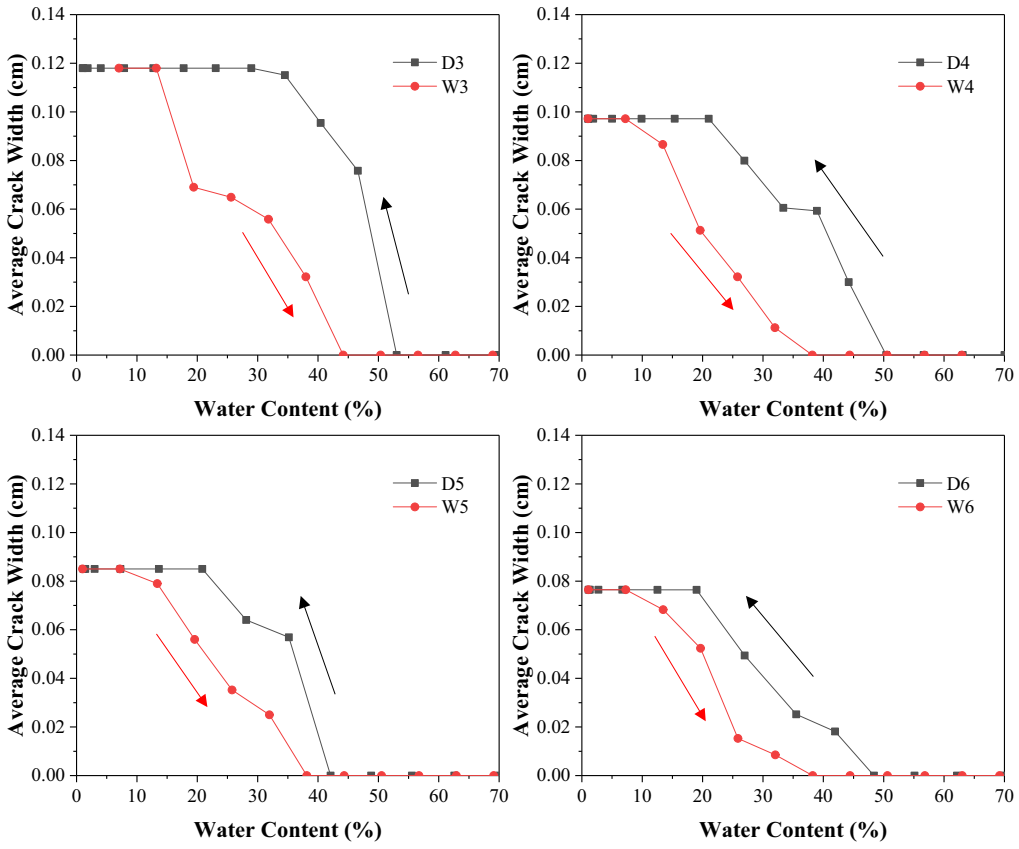

(b)

Fig. 9 The evolution of the average crack width with water content: **a** under the six drying paths and **b** during D-W cycles

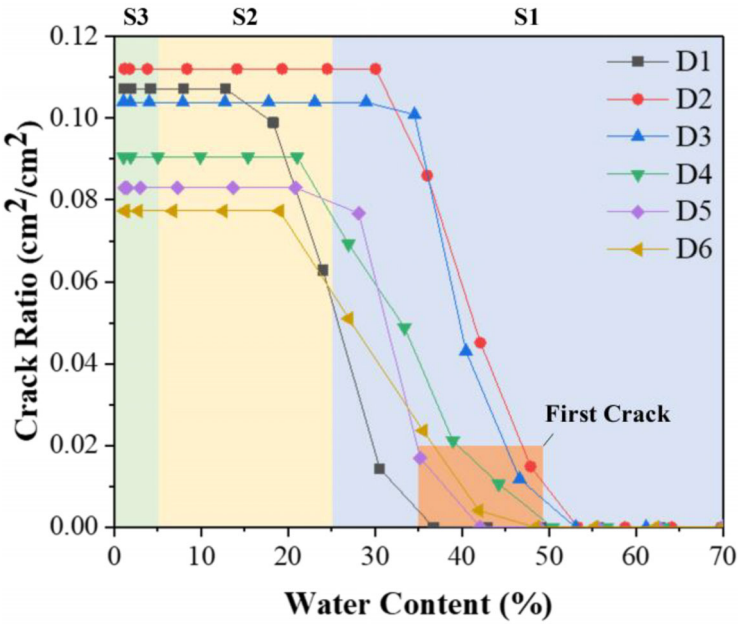

(a)

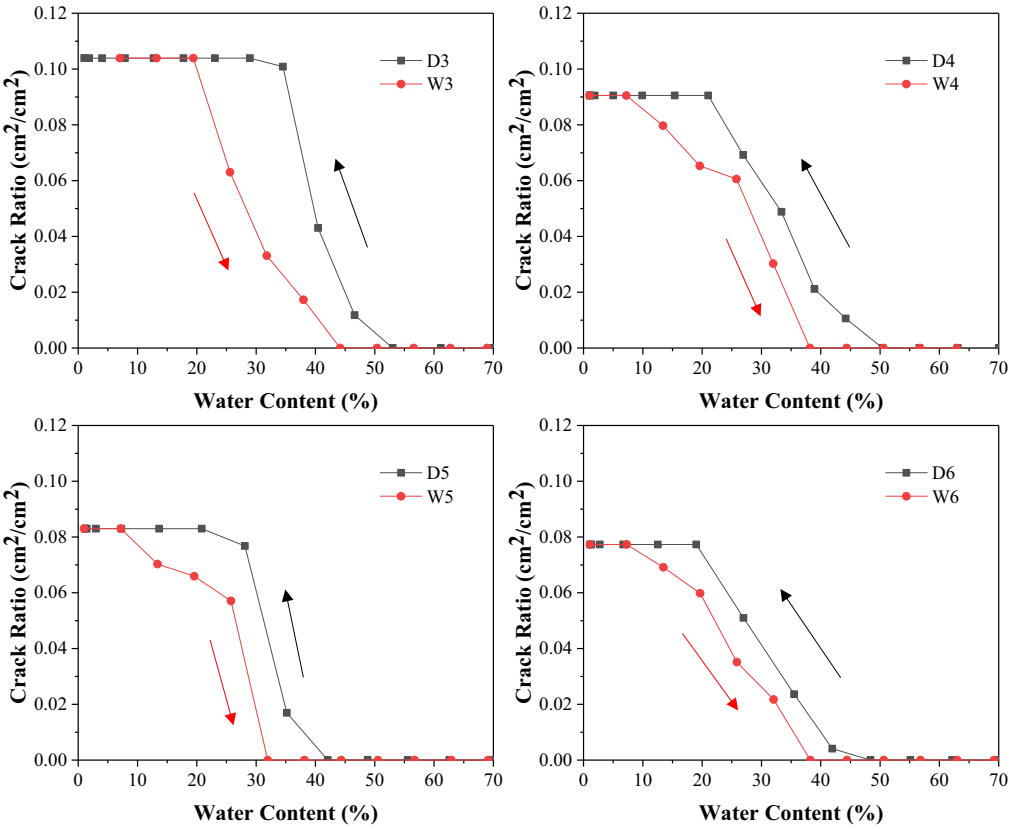

(b)

Fig. 10 (**a** The evolution of crack ratio with water content in the drying path and **b** cracking hysteresis phenomenon during D-W cycles

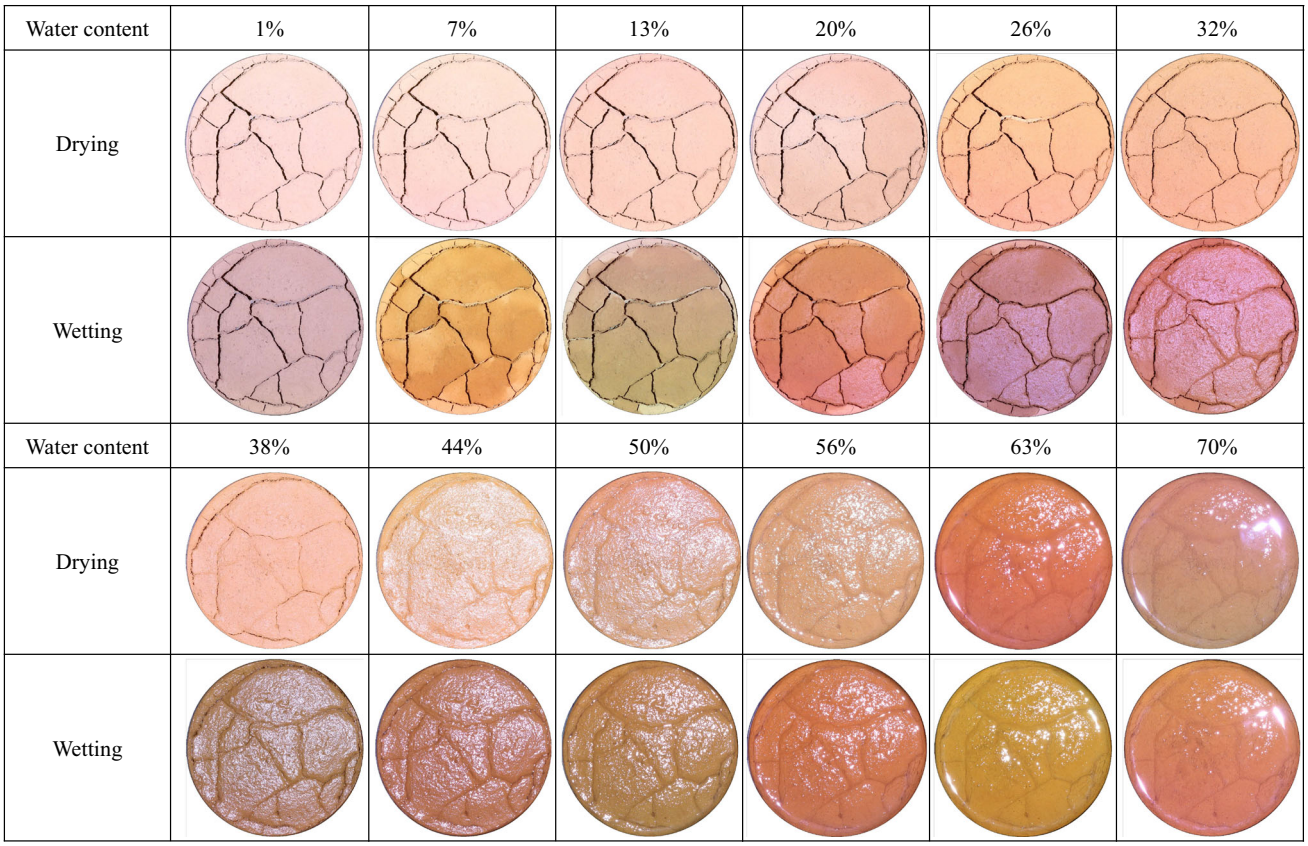

Fig. 11 Images of the soil specimen in D4 and W4 with different water contents

volumetric deformation of the soil, the 3D characterization of cracks is necessary and critical.

3.3 3D characteristics of cracked soils

The greatest advantage of using 3D characterization for the cracked soil is the detection of crack depth. Crack depth is defined by the vertical propagation distance of the surface defect [27]. Soil morphology was investigated based on 3D laser scanning, which allowed for the reconstruction of a 3D model for the cracked soil. Figure 12a shows a 2D image of the cracked soil, in which the crack depth is not visible. The 3D characterization was then conducted by showing the profile of the crack morphology in both vertical and horizontal directions, as shown in Fig. 12b. To better investigate and quantify the crack propagation, a circular zone of interest with a diameter of 3 cm on the cracked soil (Fig. 12a) was selected for 3D scanning and the corresponding 3D morphology of desiccation cracks at various D-W cycles is presented in Fig. 12b. The elevation of every planar point on the cracked soil was evaluated so that the crack depth and the volume of desiccation cracks can be estimated. The magnified images can not only capture the vertical and horizontal propagation of the crack, but also the settlement or heave of the soil during D-W cycles. As compared with the 2D characterization, more morphological details of the cracked soil were presented in the 3D scanning. Due to the desiccation, the clayed soil was undergoing shrinkage and cracking, which leads to the particle arrangement and the nonuniform volumetric change [27, 29]. For example, it is noticed that many bumps next to the primary crack were formed during D-W cycles (marked by the red arrow in Fig. 12b). These minor morphological characteristics during D-W cycles captured the change in the volume and macropore structure of the cracked soil. This shows the advantage of using 3D characterization for spatiotemporally evaluating the surface morphology of the cracked soil over 2D images.

The quantified 3D characteristics of volumetric changes in the cracked soil are shown in Fig. 13. A segment of the cracked soil was selected to quantify the crack depth and the average height of the soil (Fig. 13a). As shown in Fig. 13b, it was found that the width of primary cracks and the depth of subcracks decrease with an increase in D-W cycles. This was consistent with the visual observation in Figs. 7, 11, and 12b. It should be noted that the detected primary cracks and subcracks are categorized as macrocracks (i.e., the crack width > 0.1 mm) and the microcrack (i.e., the crack width < 0.1 mm) might not be captured due to the limited 3D scanning resolution (> 0.05 mm).

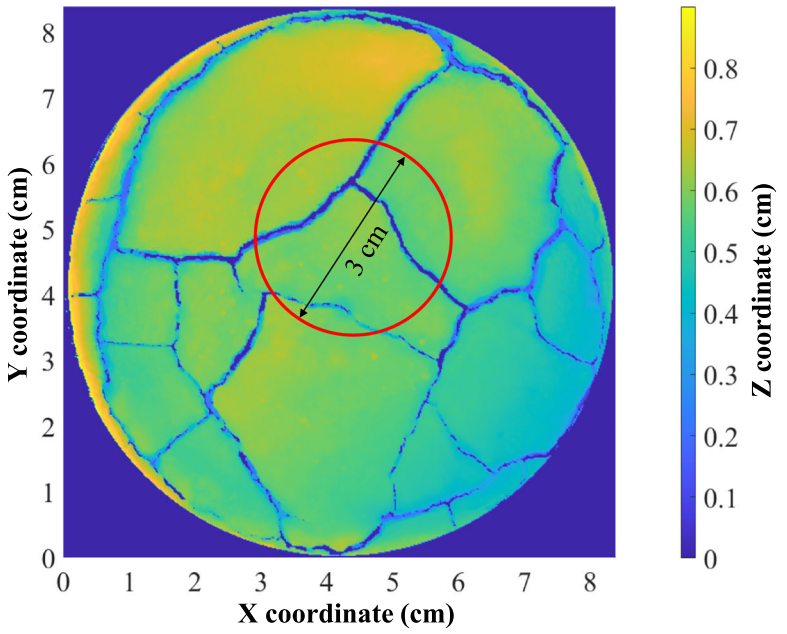

(a)

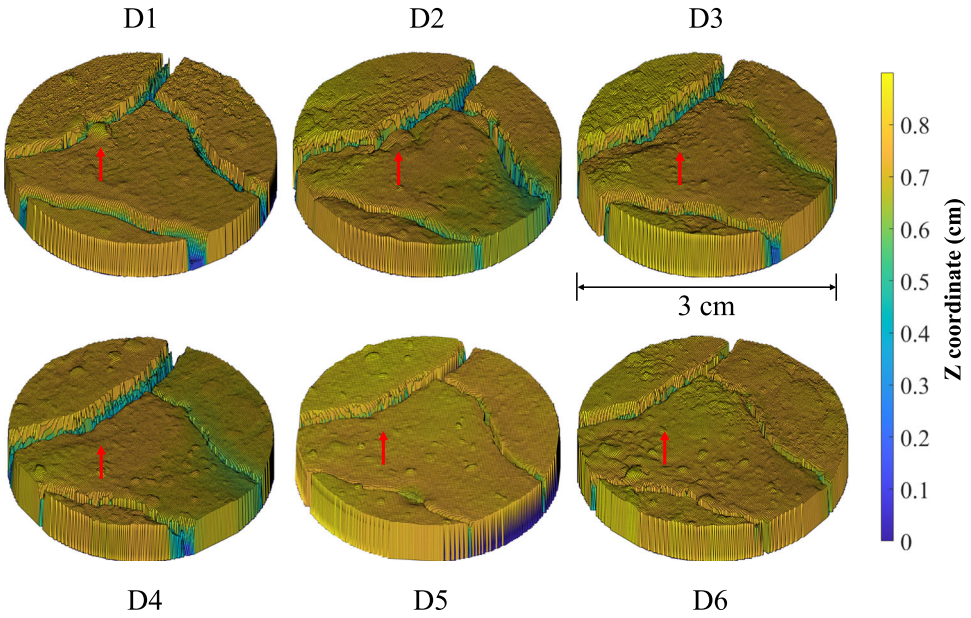

(b)

Fig. 12 Reconstructed 3D model of the selected circular area: **a** the planar view of the cracked soil and **b** the visualized 3D morphology of the crack and the soil

Nevertheless, the macroscopic volumetric behavior of the cracked soil can still be interpreted. Although the crack volume decreased during D-W cycles, the height of the soil mass increased generally, as shown in Fig. 13c. The average height of the overall sample increased by 13.3% and the average height soil increased by 24.3% after 6 D-W cycles. These characteristics are found insignificant in the 2D images, but the 3D characterization highlights the influence of D-W cycles on the macroporosity of the cracked soil. It is known that the desiccation crack is

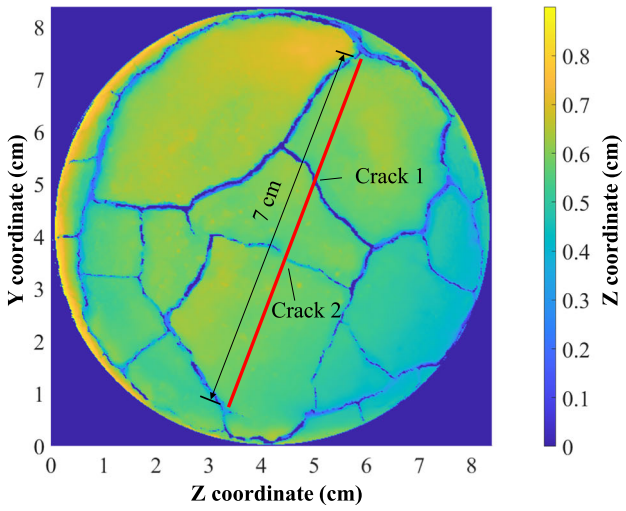

(a)

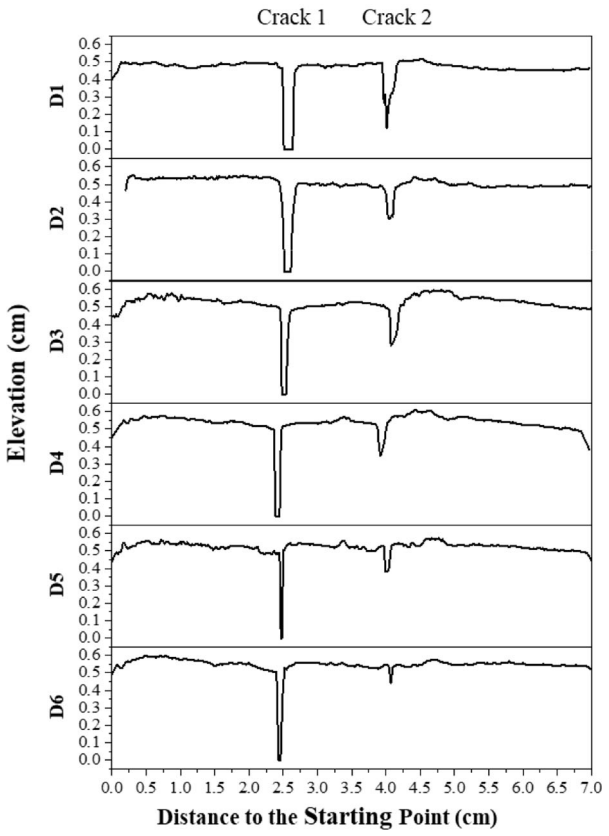

(b)

Fig. 13 Influence of D-W cycles on the volumetric change of the cracked soil: **a** the selected segment for quantification; **b** the evolution of the crack propagation; **c** the average overall and soil height at the end of each D-W cycle

triggered by the air invasion in the desiccation crack, causing the particle rearrangement near the crack [27, 36]. Under D-W cycles, the nonuniform volumetric change induced by particle rearrangement was toward the

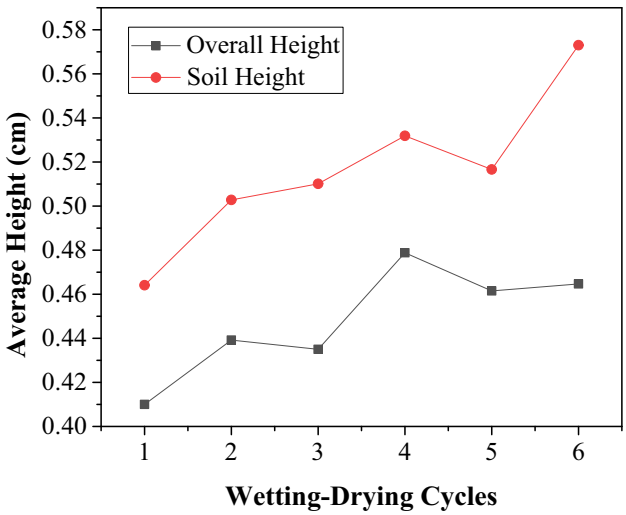

(c)

Fig. 13 continued

stabilized the pore structure of the cracked soil, causing the macroporosity loosening [29]. This led to an increase in the aggregate distance and a reduction in the macropore (> 0.075 mm) and the associated crack width/depth, consequently resulting into a subtle increase in the height of the cracked soil [29].

The 3D characteristics of the cracked soil were further interpreted by considering the surface area and the volume of desiccation cracks for the entire sample. The surface area of the soil specimen against gravimetric soil water content during D-W cycles is shown in Fig. 14. Results showed that the surface area of the cracked soil generally increased with a decrease in water content. This was attributed to the formation of desiccation cracks, which increased the area exposed to the atmosphere [22], although the desiccation would cause the soil shrinkage. This 3D characterized surface area could provide a more insightful estimation of the exposed area for predicting water evaporation of the cracked soil [22, 28], as compared to that of 2D crack ratio. The surface area increased dramatically after the first crack was triggered and became stabilized in the second stage of evaporation. The surface area at the end of the drying path increased with the D-W cycle due to the generation of subcracks, which indicates soil degradation.

The comparison of the surface area changes in the drying and wetting paths is shown in Fig. 14b. The surface area changes during the wetting process were higher than that in the drying process for a given water content. This also shows the hysteresis phenomenon of cracking characteristics in unsaturated soil [14, 40]. When the water content was relatively low (less than 20%, i.e., shrinkage limit) or high (greater than 60%, i.e., saturated water

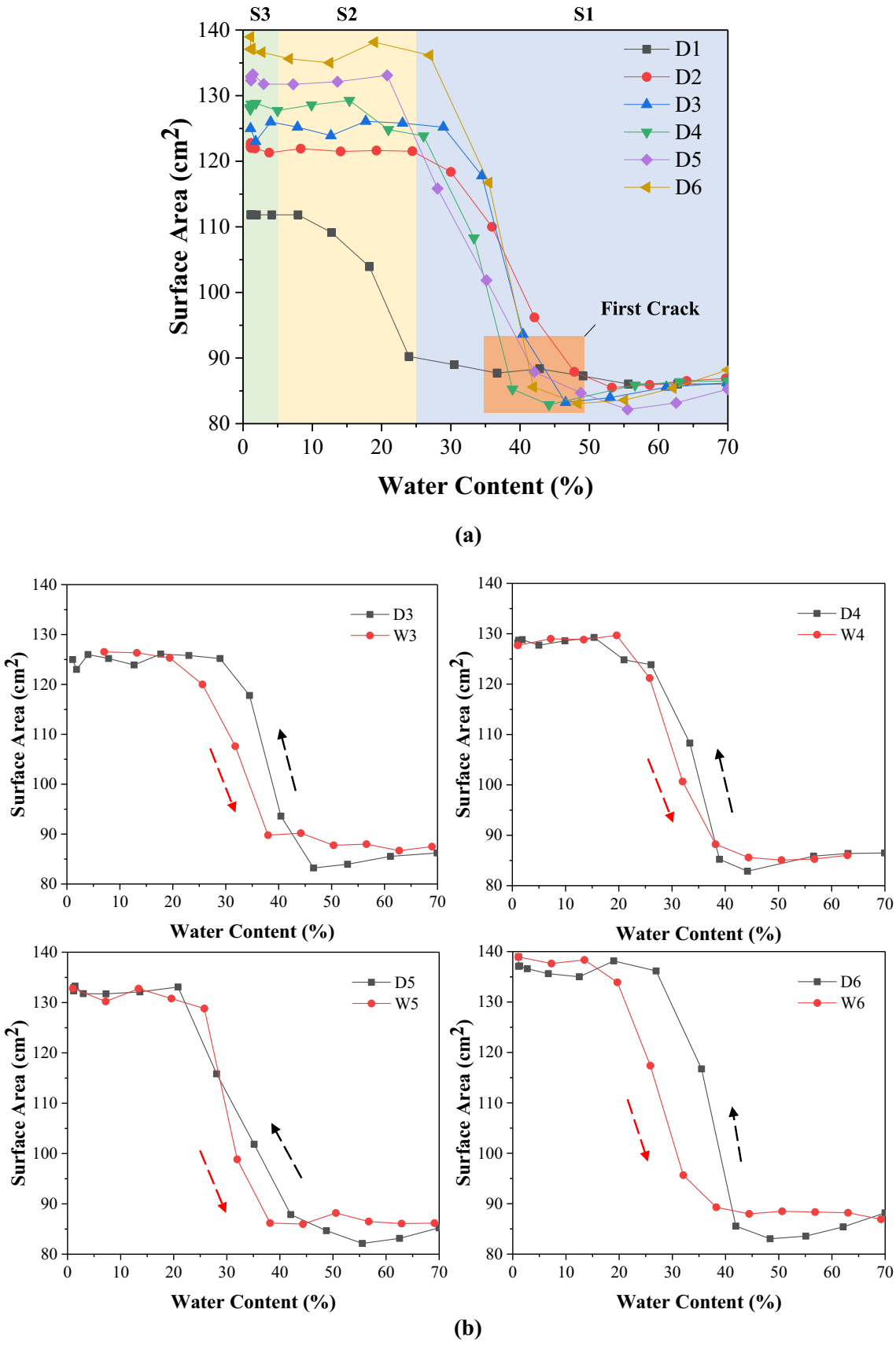

Fig. 14 The evolution of surface area with water content: **a** under the six drying processes and **b** during wetting–drying cycles

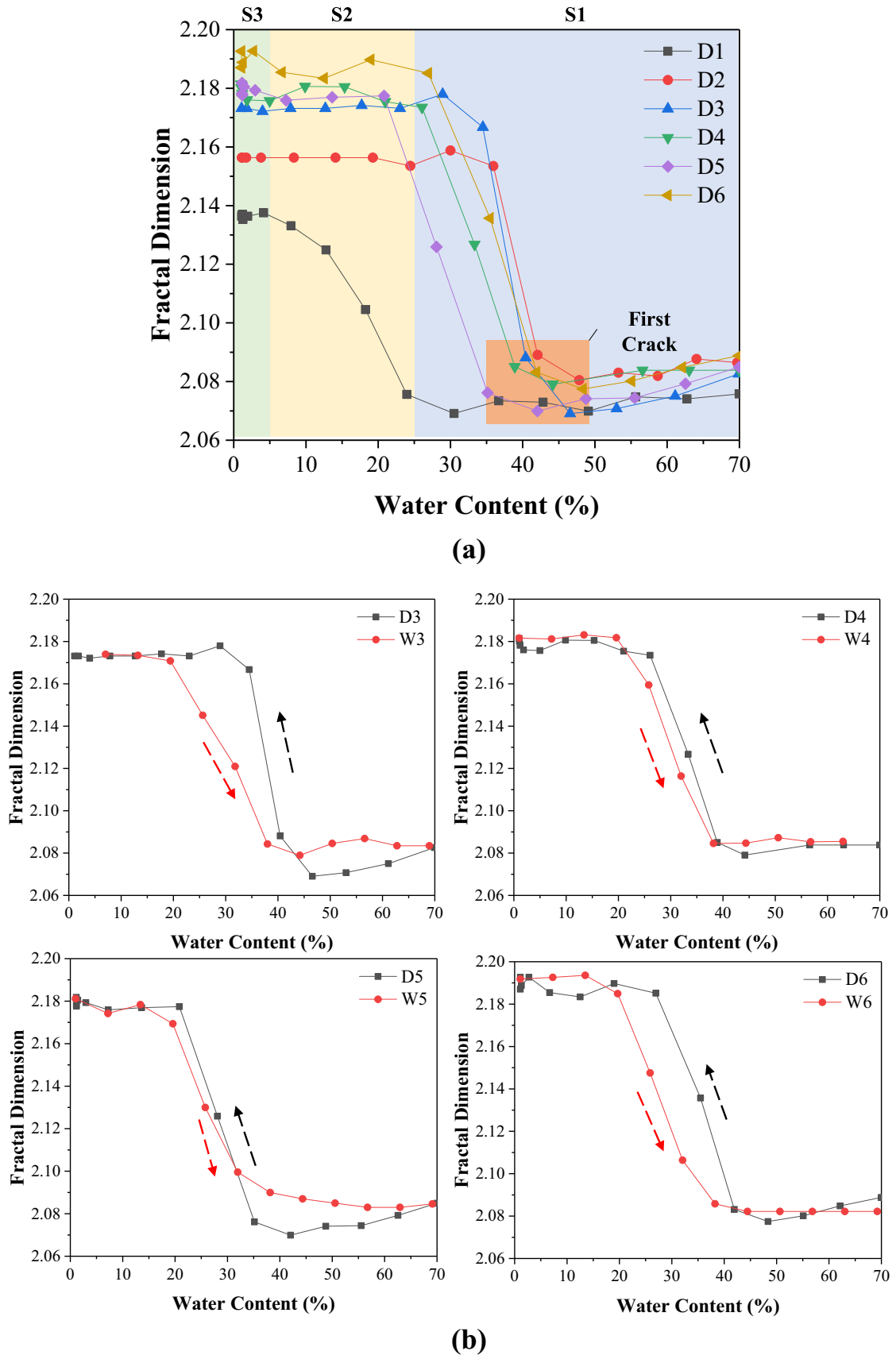

Fig. 15 The evolution of fractal dimension with water content: **a** under the six drying processes and **b** during wetting–drying cycles

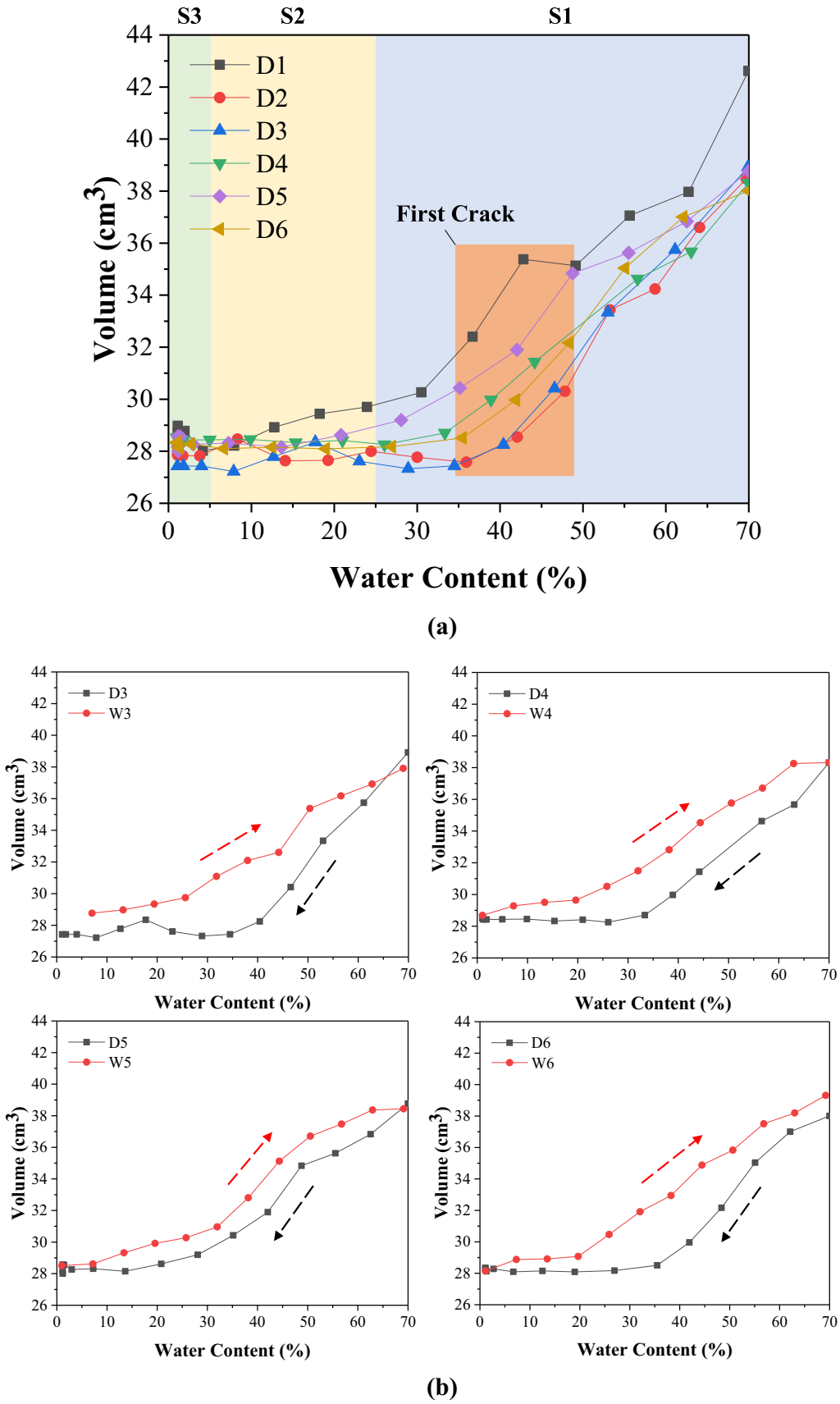

Fig. 16 The evolution of volume with water content: **a** in 6 drying paths and **b** during D-W cycles

content), the surface area of the sample in the wetting path and the drying process was very close. However, within the range between 20 and 60% of water content, the hysteresis phenomenon was pronounced, in terms of the surface area, total crack length, average crack width and crack ratio. The characteristics of the surface area in the wetting and drying process were consistent with the morphological features observed from the 2D images (Fig. 11).

Fractal dimension is a mathematical framework proposed by [17], which can characterize the heterogeneity, complexity, irregularity and self-similarity of the spatial distribution of solid and void phases. In this study, the fractal dimension was calculated by the box-counting method. The principle of this method is to use cubes with different side lengths to cover the fractal surface, then calculate the relation between the non-empty cubes and the cube size. More details about the calculation of fractal dimension can be found in our prior study [52]. Figure 15 presents the fractal dimension of the soil surface against the gravimetric water content. It was observed that the fractal dimension variation followed a similar trend with the surface area changes. The fractal dimension significantly changed after the onset of the first crack and became stable in the second stage of the evaporation. In accordance with the surface area, the final fractal dimension after each drying process increased due to the formation of new cracks. As for the comparison of fractal dimension changes in the wetting and drying process shown in Fig. 15b, the results indicate that the fractal dimension shares similar characteristics with the surface area.

The correlation between the specimen volume and water content is presented in Fig. 16. The evolution of the volume with respect to the water content was consistent with the soil characteristic shrinkage curve [32]. The volume (indicating the void ratio) of the cracked soil decreased with a decrease in the water content. Three stages (i.e., normal shrinkage, residual shrinkage, and zero shrinkage) in the soil shrinkage characteristic curve can be correspondingly found in the curves in Fig. 16. The volume first decreased linearly with the water content, and then became stabilized and independent from the water content at the end of the drying path. The final volume at the end of the drying path was found to increase with the D-W cycles. This suggests that soil degradation would be caused by the macroporosity loosing during D-W cycles [29]. Similarly, the hysteresis phenomenon of cracking characteristics in the unsaturated soil was also found in the evolution of the volume change, as shown in Fig. 16b. It should be noted that, due to the limited resolution of the structured light 3D scanner, the subsurface air voids inside the specimen cannot be precisely identified, resulting in a possible overestimation of the volume of the soil. Nevertheless, the current study provides a considerable approach to capture the shrinkage characteristic curve or swelling curve of the cracked soil.

4 Conclusions

In this study, 2D and 3D characterization techniques were adopted to capture the evolution of desiccation cracks under six wetting–drying cycles. Crack pattern parameters, such as crack ratio, average crack width, and the total crack length were analyzed by the 2D image processing. 3D soil cracking parameters, such as surface area, volume, and the fractal dimension of the cracked soil body were determined from the 3D reconstructed soil model. The interpretation of these experimental results leads to the key findings as follows:

(1) The 2D cracking characteristics based on digital photography showed that subcracks and soil degradation formed during D-W cycles, while the 3D tomography revealed the remained cracking network memory and the deterioration of pore structure during D-W cycles.
(2) The hysteresis phenomenon was found in the evolution of cracking characteristics on the water content. The crack opening in the drying path and the crack closure on the wetting path achieved different crack intensities under the same water content level. This was attributed to the hydraulic hysteresis in the soil water retention curve.
(3) This study compared the 2D and 3D characterization of desiccation cracks and it was found that the crack characteristics could be associated with the hydromechanical responses of the unsaturated clayed soil. As compared to the 2-D cracking evolution, the 3D characterization can provide a more accurate interpretation of volumetric behaviors for cracked soils in geoenvironmental infrastructures.

Acknowledgements This research is supported by the Camden Health Research Initiative of Rowan University and National Key Research and Development Program of China (Grant No. 2020YFC1808101). Undergraduate students at Rowan University, including David Spell, Lauren Blaze, and Amanda Groschadl have assisted the authors in laboratory work. Permission to publish this work was granted by the Director of Rowan University's Center for Research and Education in Advanced Transportation Engineering Systems (CREATEs). The second author (Weiling Cai) is also grateful for the support by the of U.S. Department of Education Graduate Assistance in Areas of National Need (GAANN) program (Grant Number: P200A210109). This work was also supported by a subaward from Rutgers University, Center for Advanced Infrastructure & Transportation, under Grant no. 69A3551847102 from the U.S. Department of Transportation, Office of the Assistant Secretary for Research and Technology (OST-R). Any opinions, findings, and conclusions or recommendations expressed in this publication are those of the author(s) and do not

necessarily reflect the views of Rutgers, the State University or those of the U.S. Department of Transportation, Office of the Assistant Secretary for Research and Technology (OST-R).

Funding Open access funding provided by Rowan University.

Declarations

Conflict of interest The authors wish to confirm that there are no known conflicts of interest associated with this publication.

References

1. Costa S, Kodikara J, Barbour S, Fredlund D (2018) Theoretical analysis of desiccation crack spacing of a thin, long soil layer. Acta Geotech 13(1):39–49
2. Cheng Q, Tang CS, Zeng H, Zhu C, An N, Shi B (2020) Effects of microstructure on desiccation cracking of a compacted soil. Eng Geol 265:105418
3. Diel J, Vogel H-J, Schlüter S (2019) Impact of wetting and drying cycles on soil structure dynamics. Geoderma 345:63–71
4. Eberemu AO (2013) Evaluation of bagasse ash treated lateritic soil as a potential barrier material in waste containment application. Acta Geotech 8(4):407–421
5. El-Zein A, Airey D, Yu B, Esgandani GA, Proust G, Dias-da-Costa D, Gao Y, Gan Y, Chen S (2021) Self-repair of cracks and defects in clay: a review of evidence, mechanisms, theories and nomenclature. Acta Geotech 16:3741–3760
6. Gebrenegus T, Ghezzehei TA, Tuller M (2011) Physicochemical controls on initiation and evolution of desiccation cracks in sand–bentonite mixtures: X-ray CT imaging and stochastic modeling. J Contam Hydrol 126(1–2):100–112
7. Glendinning S, Hughes P, Helm P, Chambers J, Mendes J, Gunn D, Wilkinson P, Uhlemann S (2014) Construction, management and maintenance of embankments used for road and rail infrastructure: implications of weather induced pore water pressures. Acta Geotech 9(5):799–816
8. Gui Y, Hu W, Zhao Z, Zhu X (2018) Numerical modelling of a field soil desiccation test using a cohesive fracture model with Voronoi tessellations. Acta Geotech 13(1):87–102
9. Hirmas DR, Giménez D, Mome Filho EA, Patterson M, Drager K, Platt BF, Eck DV (2016) Quantifying soil structure and porosity using three-dimensional laser scanning. Digital soil morphometrics. Springer, Berlin, pp 19–35
10. Jentsch A, Beierkuhnlein C (2008) Research frontiers in climate change: effects of extreme meteorological events on ecosystems. CR Geosci 340(9–10):621–628
11. Julina M, Thyagaraj T (2019) Quantification of desiccation cracks using X-ray tomography for tracing shrinkage path of compacted expansive soil. Acta Geotech 14(1):35–56
12. Khaddour G, Riedel I, Andò E, Charrier P, Bésuelle P, Desrues J, Viggiani G, Salager S (2018) Grain-scale characterization of water retention behaviour of sand using X-ray CT. Acta Geotech 13:497–512
13. Li J, Zhang L (2011) Study of desiccation crack initiation and development at ground surface. Eng Geol 123(4):347–358
14. Li JH, Zhang LM, Li X (2011) Soil-water characteristic curve and permeability function for unsaturated cracked soil. Can Geotech J 48(7):1010–1031
15. Liu C, Tang CS, Shi B, Suo WB (2013) Automatic quantification of crack patterns by image processing. Comput Geosci 57:77–80
16. Louati F, Trabelsi H, Jamei M, Taibi S (2018) Impact of wetting-drying cycles and cracks on the permeability of compacted clayey soil. Eur J Environ Civ Eng 25(4):696–721
17. Mandelbrot BB (1982) The fractal geometry of nature. WH freeman, New York
18. Miralles DG, Teuling AJ, Van Heerwaarden CC, De Arellano JV-G (2014) Mega-heatwave temperatures due to combined soil desiccation and atmospheric heat accumulation. Nat Geosci 7(5):345–349
19. Nahlawi H, Kodikara JK (2006) Laboratory experiments on desiccation cracking of thin soil layers. Geotech Geol Eng 24(6):1641–1664
20. Peron H, Hueckel T, Laloui L, Hu L (2009) Fundamentals of desiccation cracking of fine-grained soils: experimental characterisation and mechanisms identification. Can Geotech J 46(10):1177–1201
21. Peron H, Laloui L, Hu L-B, Hueckel T (2013) Formation of drying crack patterns in soils: a deterministic approach. Acta Geotech 8(2):215–221
22. Poulsen TG, Cai W, Garg A (2020) Water evaporation from cracked soil under moist conditions as related to crack properties and near-surface wind speed. Eur J Soil Sci 71(4):627–640
23. Qi W, Zhang ZY, Wang C (2020) Desiccation and cracking behaviour of clay loam subjected to different irrigation methods during wetting–drying cycles. Eur J Soil Sci 72(2):793–809
24. Rayhani MH, Yanful E, Fakher A (2007) Desiccation-induced cracking and its effect on the hydraulic conductivity of clayey soils from Iran. Can Geotech J 44(3):276–283
25. Rodríguez R, Sanchez M, Ledesma A, Lloret A (2007) Experimental and numerical analysis of desiccation of a mining waste. Can Geotech J 44(6):644–658
26. Sanchez M, Atique A, Kim S, Romero E, Zielinski M (2013) Exploring desiccation cracks in soils using a 2D profile laser device. Acta Geotech 8(6):583–596
27. Shin H, Santamarina JC (2011) Desiccation cracks in saturated fine-grained soils: particle-level phenomena and effective-stress analysis. Géotechnique 61(11):961–972
28. Song WK, Cui YJ (2020) Modelling of water evaporation from cracked clayey soil. Eng Geol 266:105465
29. Sun H, Mašín D, Najser J, Neděla V, Navrátilová E (2019) Bentonite microstructure and saturation evolution in wetting–drying cycles evaluated using ESEM. MIP WRC Meas Géotech 69(8):713–726
30. Tang AM, Vu M, Cui Y-J (2011) Effects of the maximum soil aggregates size and cyclic wetting–drying on the stiffness of a lime-treated clayey soil. Géotechnique 61(5):421–429
31. Tang CS, Cheng Q, Leng T, Shi B, Zeng H, Inyang HI (2020) Effects of wetting-drying cycles and desiccation cracks on mechanical behavior of an unsaturated soil. CATENA 194:104721

32. Tang C-S, Cui Y-J, Shi B, Tang A-M, Liu C (2011) Desiccation and cracking behaviour of clay layer from slurry state under wetting–drying cycles. Geoderma 166(1):111–118
33. Tang CS, Shi B, Liu C, Suo WB, Gao L (2011) Experimental characterization of shrinkage and desiccation cracking in thin clay layer. Appl Clay Sci 52(1–2):69–77
34. Tang C-S, Zhu C, Cheng Q, Zeng H, Xu J-J, Tian B-G, Shi B (2021) Desiccation cracking of soils: a review of investigation approaches, underlying mechanisms, and influencing factors. Earth-Sci Rev 216:103586
35. Tay Y, Stewart D, Cousens T (2001) Shrinkage and desiccation cracking in bentonite–sand landfill liners. Eng Geol 60(1–4):263–274
36. Tran KM, Bui HH, Kodikara J, Sánchez M (2020) Soil curling process and its influencing factors. Can Geotech J 57(3):408–422
37. Vail M, Zhu C, Tang C-S, Anderson L, Moroski M, Montalbo-Lomboy MT (2019) Desiccation cracking behavior of MICP-treated bentonite. Geosciences 9(9):385
38. Viggiani G, Andò E, Takano D, Santamarina JC (2015) Laboratory X-ray tomography: a valuable experimental tool for revealing processes in soils. Geotech Test J 38(1):61–71
39. Wan Y, Xue Q, Liu L (2014) Study on the permeability evolution law and the micro-mechanism of CCL in a landfill final cover under the dry-wet cycle. Bull Eng Geol Env 73(4):1089–1103
40. Wang C, Zhang Z-y, Liu Y, Fan S-m (2017) Geometric and fractal analysis of dynamic cracking patterns subjected to wetting-drying cycles. Soil Tillage Res 170:1–13
41. Wang C, Zhang Z-y, Qi W, Fan S-m (2018) Morphological approach to quantifying soil cracks: application to dynamic crack patterns during wetting-drying cycles. Soil Sci Soc Am J 82(4):757–771
42. Wang L-L, Tang C-S, Shi B, Cui Y-J, Zhang G-Q, Hilary I (2018) Nucleation and propagation mechanisms of soil desiccation cracks. Eng Geol 238:27–35
43. Wang JP, Lambert P, De Kock T, Cnudde V, François B (2019) Investigation of the effect of specific interfacial area on strength of unsaturated granular materials by X-ray tomography. Acta Geotech 14:1545–1559
44. Wang JP, Luan JY, Gao XG, Liu TH, Ando E, François B (2022) A micro-investigation of unsaturated sand in mini-triaxial compression based on micro-CT image analysis. Acta Geotech 17(11):4799–4821
45. Wang P, Guo X, Sang Y, Shao L, Yin Z, Wang Y (2020) Measurement of local and volumetric deformation in geotechnical triaxial testing using 3D-digital image correlation and a subpixel edge detection algorithm. Acta Geotech 15:2891–2904
46. Wijaya M, Leong EC, Rahardjo H (2015) Effect of shrinkage on air-entry value of soils. Soils Found 55(1):166–180
47. Wilson GW, Fredlund D, Barbour S (1994) Coupled soil-atmosphere modelling for soil evaporation. Can Geotech J 31(2):151–161
48. Xie Y, Costa S, Zhou L, Kandra H (2020) Mitigation of desiccation cracks in clay using fibre and enzyme. Bull Eng Geol Env 79(8):4429–4440
49. Yilmaz I (2006) Indirect estimation of the swelling percent and a new classification of soils depending on liquid limit and cation exchange capacity. Eng Geol 85(3–4):295–301
50. Zaidi M, Ahfir ND, Alem A, Taibi S, Mansouri B, Zhang Y, Wang H (2021) Use of X-ray computed tomography for studying the desiccation cracking and self-healing of fine soil during drying–wetting paths. Eng Geol 292:106255
51. Zhao B, Santamarina JC (2020) Desiccation crack formation beneath the surface. Géotechnique 70(2):181–186
52. Zhuo Z, Zhu C, Tang C-S, Xu H, Shi X, Mark V (2022) 3D characterization of desiccation cracking in clayey soils using a structured light scanner. Eng Geol 299:106566